Homoleptic purine-based NHC iridium(iii) complexes for blue OLED application: impact of isomerism on photophysical properties

Armands Sebris, Matas Guzauskas, Malek Mahmoudi, Dmytro Volyniuk, Juozas V Grazulevicius, Anatoly Mishnev, Irina Novosjolova, Māris Turks, Gediminas Jonusauskas, Kaspars Traskovskis

Homoleptic purine-based NHC iridium(III) complexes for blue OLED application: impact of isomerism on photophysical properties

Armands Sebris,[a] Matas Guzauskas,[b] Malek Mahmoudi,[b] Dmytro Volyniuk,[b] Juozas V. Grazulevicius,[b] Anatoly Mishnev,[c] Irina Novosjolova,[a] Māris Turks,[a] Gediminas Jonusauskas[d] and Kaspars Traskovskis[e]

With a motivation to develop deep-blue emitters for organic light-emitting diodes (OLEDs) stereoisomers of a homoleptic N-heterocyclic carbene (NHC) iridium(III) complex bearing 7,9-dihydro-8*H*-purin-8-ylidene ligands (***mer*-PhP** and ***fac*-PhP**) have been synthesized and their photophysical, electrical and electroluminescent properties investigated. The studied complexes only transport holes with the highest hole mobility value of 2×10^{-4} cm^2 V^{-1} s^{-1} at an electric field of 4.9×10^5 V cm^{-1} in the case of ***fac*-PhP**. When molecularly dispersed in PMMA films, the compounds show bright blue phosphorescence (466 and 437 nm) with photoluminescence quantum yield (Φ_{PL}) values of 0.99 and 0.77. The complexes also possess exceptional thermal stability with a 5% mass loss point at up to 480 °C. While the *mer*-isomer shows more efficient photoluminescence and a twofold higher radiative rate, it is more sensitive to external stimulus: its Φ_{PL} significantly drops and an emission redshift takes place upon transfer from a rigid to liquid surrounding medium or under exposure to a temperature increase. DFT calculations relate this effect to a weakened metal–ligand bonding at the lowest energy excited triplet state (T_1) of the compound, which promotes the extent of non-radiative relaxation processes. On the basis of ***mer*-PhP** an efficient blue OLED was prepared with an emission maximum wavelength of 467 nm and a maximum external quantum efficiency of 16.1%.

Introduction

The last two decades have witnessed significant advances in organic light emitting diode (OLED) technology with the most prominent beneficiary of this being the display industry, which has subsequently delivered innovative products with unmatched image quality and previously inaccessible functionality, such as transparency and flexibility.[1–4] Phosphorescent cyclometalated iridium(III) complexes are the leading commercialized light emitting OLED material class due to the ability of providing efficient light emission from the triplet excited states, characterized with large photoluminescence quantum yield values (Φ_{PL}) and few microsecond long emission lifetimes (τ).[5–8] Despite the fact that iridium(III) based emitters are extensively used for providing light in green and red spectral regions, the development of blue phosphorescent materials is still an unresolved challenge.[9] The main culprit of the existing structures is insufficient chemical stability, which results in short operational lifetimes of the blue OLEDs.

A widespread strategy towards attaining blue emitting iridium(III) complexes involves an attachment of electron accepting groups at the cyclometalating ligands. The introduction of fluorine atoms is one of the commonly used approaches, as seen in the quintessential blue emitter FIrpic.[10] However, the experimental observations show that a detachment of fluorine atoms in the excited states of molecules is a common in-device degradation pathway of such materials.[11] Besides intraligand bond cleavage, metal–ligand dissociation is the other widely encountered degradation mechanism of iridium(III) phosphors. This is related to the high energies of the blue-emitting metal-to-ligand charge transfer triplet levels (^{3}MLCT), which place

[a] *Institute of Technology of Organic Chemistry, Faculty of Materials Science and Applied Chemistry, Riga Technical University, P. Valdena Str. 3, LV-1048, Riga, Latvia*
[b] *Department of Polymer Chemistry and Technology, Kaunas University of Technology, Barsausko 59, LT- 51423, Kaunas, Lithuania*
[c] *Latvian Institute of Organic Synthesis, Aizkraukles Str. 21, Riga, LV-1006, Latvia*
[d] *Laboratoire Ondes et Matière d'Aquitaine, Bordeaux University, UMR CNRS 5798, 351 Cours de la Libération, 33405 Talence, France*
[e] *Institute of Applied Chemistry, Faculty of Materials Science and Applied Chemistry, Riga Technical University, P. Valdena Str. 3, LV-1048, Riga, Latvia. E-mail: kaspars.traskovskis@rtu.lv*

them in close energetic proximity to the metal centered (^{3}MC) excited states.[12] Upon the population of MC levels, the geometries of complexes transform through a partial dissociation of ligands. Such a process may not only lead to a complete ligand dissociation, but is also associated with a severe drop in Φ_{PL} values because ^{3}MC levels are considered to be non-emissive.[12] One of the proposed structural strategies towards making iridium(III) complexes more resilient is a substitution of the relatively weak metal–nitrogen (Ir–N:) bonds with stronger metal–carbene (Ir–C:) analogues. Due to sturdier ligand bounding ^{3}MC states in the corresponding complexes being less accessible and, even if populated, a reverse ^{3}MC → ^{3}MLCT pathway in the excited state configuration may be possible for the mentioned emitters.[12–14] Following this concept numerous successful blue-emitting iridium(III) molecular designs have been developed, where the chemical composition of the emitters involves the use of N-heterocyclic carbene (NHC) building blocks. The first structural examples of such emitters featured ligands bearing imidazol-2-yl and benzimidazol-2-yl,[15,16] or pyridylimidazol-2-yl[17] NHC fragments. However, the disadvantage of these early NHC-based emissive materials is their high triplet energies, which complicate OLED preparation due to the lack of suitable charge transporting host materials. The introduction of an additional nitrogen atom to the pyridylimidazole ring system stabilizes the LUMO level of the corresponding compounds and redshifts their emission, resulting in more robust devices, as seen in the case of pyrazinoimidazol-2-yl ligand containing emitters.[18–20] Very recently another closely related NHC-type ligand was introduced in the form of 7,9-dihydro-8*H*-purin-8-ylidene. Structural examples *f*-2*t*Bu, *m*-2*t*Bu,[21] *f*-CF_3 and *f*-$PhCF_3$[22] (Fig. 1) exhibit blue emission with exceptional Φ_{PL} values and good OLED performance. A common structural characteristic of the mentioned compounds is the presence of bulky alkyl substituents at the aromatic rings of the cyclometalating ligands. Bulky groups are known to provide some benefit in the form of preventing close contact between the emitter molecules in the emissive layers of OLEDs, thus minimizing the extent of such negative molecular aggregation-induced effects such as luminescence concentration quenching and triplet–triplet annihilation,[23,24] yet, there are several drawbacks. Alkyl substituents possess weak electron donating properties, which are known to redshift the emission wavelength and reduce the Φ_{PL} of the corresponding complexes.[25] Bulky groups may also block charge carrier transport to emitter molecules, reducing the overall electroluminescence performance.[26,27] Another disadvantage is the increased molecular mass of the compounds, which negatively affects their thermal stability and may facilitate partial material degradation during the vacuum deposition stage of OLED preparation.

In this work, after developing a successful synthetic pathway to unsubstituted 7-methyl-9-phenyl-9*H*-purin-7-ium ligand precursor, we present two stereoisomers of the corresponding homoleptic complex, ***mer*-PhP** and ***fac*-PhP** (Fig. 1). The compounds show strong emission in the blue spectral region with Φ_{PL} values up to 0.99. Comprehensive photophysical and theoretical characterization of light emission processes reveal striking differences in emission characteristics between the two investigated stereoisomers in terms of emission efficiency, emissive rate constants and response to the surrounding medium. The compounds were successfully integrated in blue

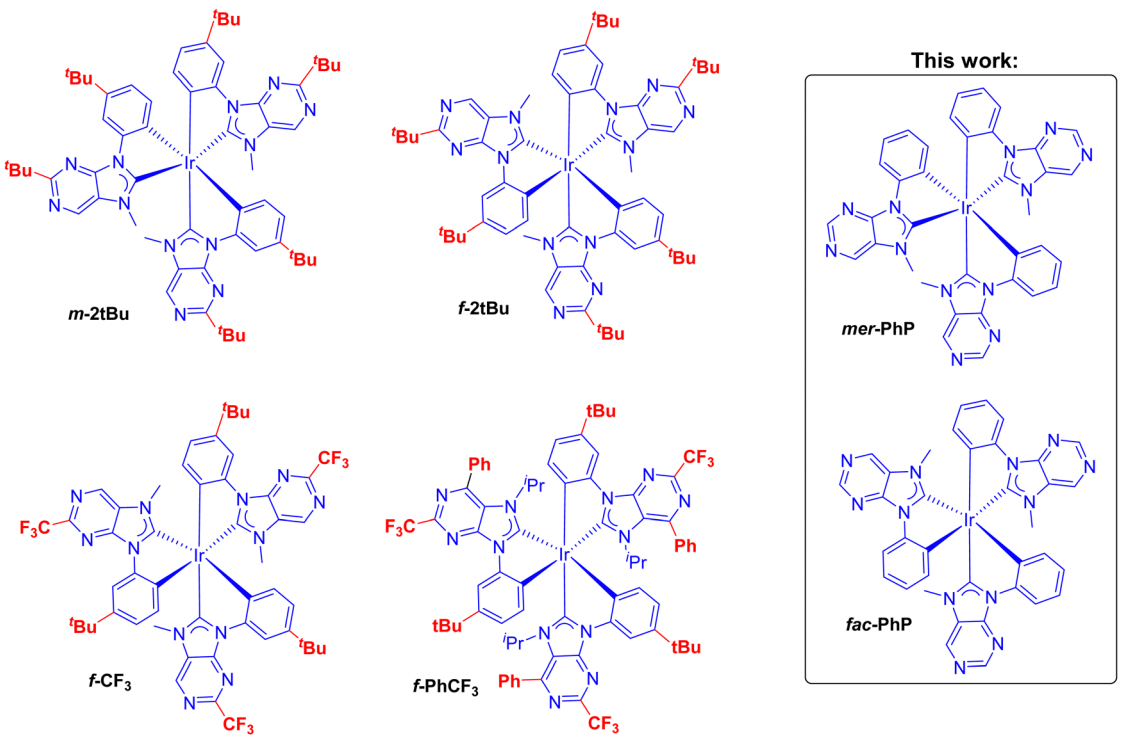

Fig. 1 Chemical structures of known[21,22] and newly synthesized 7,9-dihydro-8*H*-purin-8-ylidene based iridium(III) complexes.

OLEDs with ***mer*-PhP** exhibiting the best performance with an external quantum efficiency (EQE) of 16.1% and emission wavelength maximum of 467 nm.

Results and discussion

Synthesis

For the initial attempts towards carbene precursor **5** (Scheme 1) methylation of the *N*(7) position of purine ring was selected. However, methylation of 9-phenylpurine and 9-phenyladenine using methyl iodide occurred selectively at the *N*(1) position, similar to reactions for structure analogs reported in the literature.[28–30] Attempts to produce the desired product using 6-chloro-9-phenylpurine and 6-cyano-9-phenylpurine[31] as starting materials were unsuccessful. Steric hindrance in the pyrimidine ring next to the *N*(1) position was suggested as a means to achieve *N*(7) alkylation in some literature sources.[21,22] However, we did not pursue this approach as it would have resulted in large alkyl groups on the end product with little benefit to the photophysical properties. Also 6-hydroxy and 6-alkoxyimino purine derivatives have been reported to undergo selective *N*(7) alkylation,[29,32] but this approach would require multiple functionalization steps on rather sensitive pyrimidoimidazolium derivatives, which are highly prone to hydrolysis towards structures of type **6**. To limit the aforementioned issues, we designed a *de novo* synthetic pathway towards ligand precursor **5** with imidazolium cation formation as the last step – right before the iridium complex formation.

Methylated compound **2** was synthesized from compound **1** using established literature protocols.[33] An aminophenyl group was introduced in the symmetrical compound **2** *via* S_NAr reaction and compound **3** was obtained as the major product. According to our observations, 70 °C was the optimal temperature for this reaction, since only minimal amounts of disubstituted product were observed and the reaction proceeded at a reasonable rate. Electronic effects, such as additional electron-donating groups in the pyrimidine ring, hindered the formation of the disubstituted product in further S_NAr reactions.[34] Pd catalyzed hydro dehalogenation with formic acid additive yielded compound **4** in high yield. Imidazolium ring closure towards compound **5** was achieved in anhydrous acidic conditions using orthoformate, although an amount of compound **6** and 8-oxopurine derivative were formed as byproducts. Based on previous observations,[35] the optimal conditions for the synthesis of iridium complex ***mer*-PhP** involved the use of AgOAc without the addition of extra bases. Alternatively, Ag_2O and a base additive (triethylamine) were also tested,[20] but compound ***mer*-PhP** was not observed. In our hands, the complex formation with ligand precursor **5** provided exclusively *mer*-isomer, while other reports regarding a few purine iridium complexes often produced a mixture of both *mer*- and *fac*-isomers requiring flash chromatography for separation.[21,22] Next, *fac*-isomer ***fac*-PhP** was achieved through trifluoroacetic acid-catalyzed isomerization similarly to a previously described methodology.[36] However, we had to add additional DCM (EtOAc:DCM = 2 : 1) to address issues related to solubility. The isomerization reaction eventually slowed down, and we did not continue it to reach full conversion as we also noticed minor simultaneous degradation.

Both iridium complexes were characterized by mass spectrometry, ^1H and ^{13}C NMR spectra. As expected for the *mer*-isomer all 3 ligands possessed NMR signals with different chemical shifts, while for the *fac*-isomer all 3 ligands had identical chemical shifts, owing to the symmetrical nature of the complex. The description of synthetic procedures and compound characterization data are provided in the ESI.†

Structure

Single crystals of ***mer*-PhP** and ***fac*-PhP** were obtained by slow evaporation of a DCM/MeOH mixture. X-ray crystallographic measurements of these samples confirmed the assumed structural composition of the two cyclometalated complexes, revealing isomers with either *mer*- or *fac*-configuration (Fig. 2). Although the octahedral configuration of ***fac*-PhP** predetermines a structure with C_3 symmetry, the geometry of the compound in crystal form deviates from the ideal case, as illustrated by slight alternations in carbon–metal bond length across three phenylpurine fragments. Distinctive differences can be seen in Ir–C bonding, whether bond-forming carbon is either carbenic (C1, C3, C5) or comes from a phenyl ring

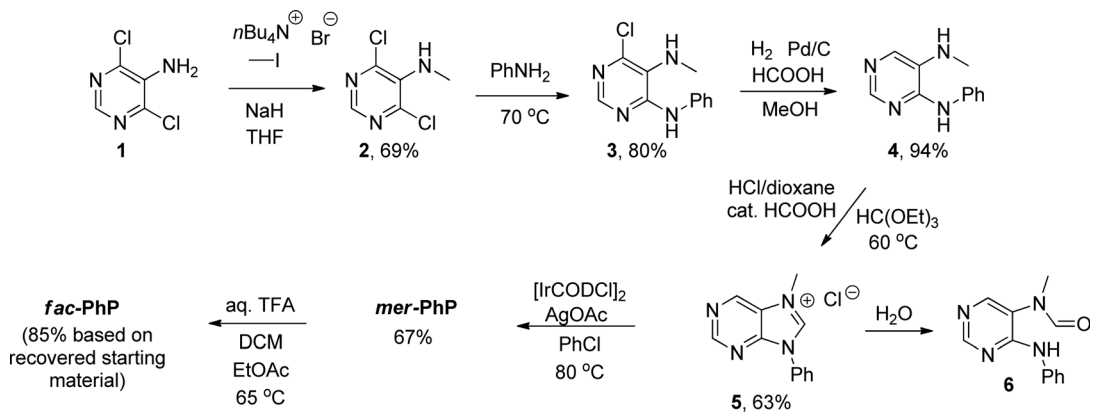

Scheme 1 The synthetic route towards purine-iridium complexes ***mer*-PhP** and ***fac*-PhP**.

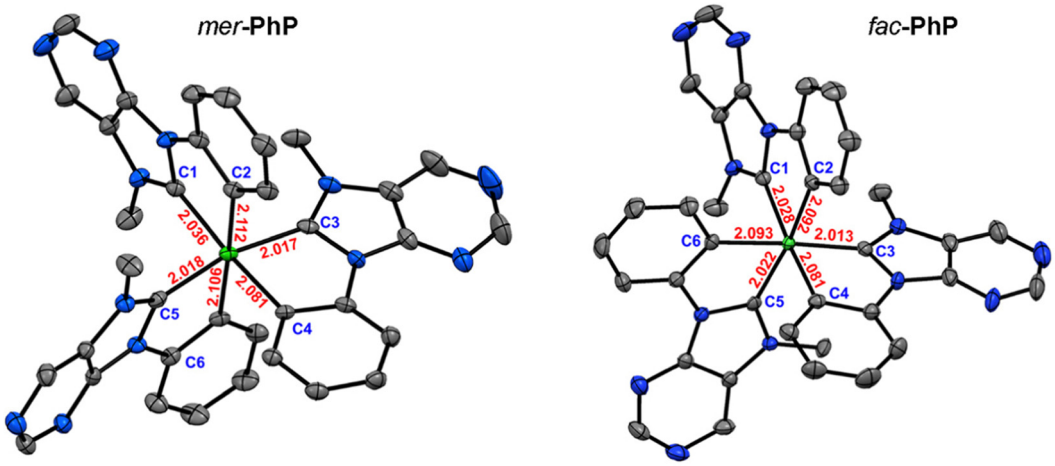

Fig. 2 X-ray structures of ***mer*-PhP** and ***fac*-PhP**. Thermal ellipsoids are drawn at the 50% probability level. Hydrogen atoms and solvent molecules are omitted for clarity.

(C2, C4, C6). In the first case the bonds are notably shorter (2.013–2.028 Å *vs.* 2.081–2.093 Å). This observation can be reasoned with the presumed backbonding between the carbenic carbon and iridium, where d_π electrons of the metal interact with an empty p orbital of the carbon, leading to shorter and more stable covalent interactions.[37] The structure of ***mer*-PhP** assumes C_1 symmetry. Bond lengths here exhibit a greater variance due to the octahedral structure featuring *trans*-positioned Ir–C bond pairs of either carbenic–carbenic (C3 and C5, 2.017, 2.018 Å), carbenic-phenyl (C1 and C4, 2.028, 2.081 Å) or phenyl–phenyl (C2 and C6, 2.112, 2.106 Å) origin. It can be seen that in the last case the metal–ligand interatomic distance is the longest. Similar observations have been made for several *mer* configured cyclometalated Ir(III) complexes and are attributed to the destabilizing *trans* effect of phenyl-type ligands.[38] Compared to the previously reported derivatives of purinylidene Ir(III) complexes, the structural characteristics of ***mer*-PhP** and ***fac*-PhP** are comparable, although we note a slight shortening of metal–ligand bonds, which might be indicative of higher chemical stability of the compounds.[21,22]

Thermal properties

The thermal properties of the synthesized compounds including their thermal stability and morphological properties were studied through thermogravimetric analysis (TGA) and differential scanning calorimetry (DSC) under a nitrogen stream.

***mer*-PhP** possesses exceptional thermal stability with a five percent weight-loss temperature ($T_{d\text{-}5\%}$) of 480 °C which is higher than $T_{d\text{-}5\%}$ of 402 °C for ***fac*-PhP**. To the best of our knowledge, *mer*-isomer exhibits the highest thermal stability among reported NHC-based iridium(III) emitters

The residue mass of the ***mer*-PhP** and ***fac*-PhP** after heating to 800 °C is 23.5% and 22.1, respectively. DSC measurements show that the investigated ***mer*-PhP** sample is an amorphous solid since temperature scans between −20 °C and 450 °C with a heating rate of 10 °C min^{-1} show no peaks associated with melting or crystallization. Similar solid state phase behavior can be observed for ***fac*-PhP**.

Photophysical properties

The results of photophysical measurements for ***mer*-PhP** and ***fac*-PhP** are summarized in Table 1. UV-Vis measurements of the complexes were carried out for DCM solution. Both compounds show strong absorbance bands in the 250–330 nm range, attributed to the ligand centered π–π* electronic transitions (Fig. 3a and b). The region of 330–425 nm is covered by

Table 1 Photophysical properties of ***mer*-PhP** and ***fac*-PhP**

Compound	λ_{abs}, nm	$\lambda_{em\ max}$, nm	Φ_{PL}	FWHM, nm	τ, ns	k_r,[a] 1×10^5 s^{-1}	k_{nr},[b] 1×10^5 s^{-1}
DCM and TOL solution							
***mer*-PhP DCM**	315, 357 (shoulder)	540	0.12	141	353	3.4	24.9
***fac*-PhP DCM**	308, 336 (shoulder)	466	0.36	94	532	6.8	12.0
***mer*-PhP TOL**	—	492	0.4	85	790	5.1	7.6
***fac*-PhP TOL**	—	436	0.22	66	400	5.5	19.5
PMMA and PS films (5 wt%)							
***mer*-PhP PMMA**	—	466	0.99	94	880	11.3	0.1
***fac*-PhP PMMA**	—	437	0.77	76	940 (60%), 2226 (40%)	5.3[c]	1.6[c]
***mer*-PhP PS**	—	470	—	81	480	—	—
***fac*-PhP PS**	—	430	—	63	630	—	—

[a] $k_r = \Phi_{PL}/\tau$. [b] $k_{nr} = (1 - \Phi_{PL})/\tau$. [c] Calculated using intensity averaged PL lifetime.

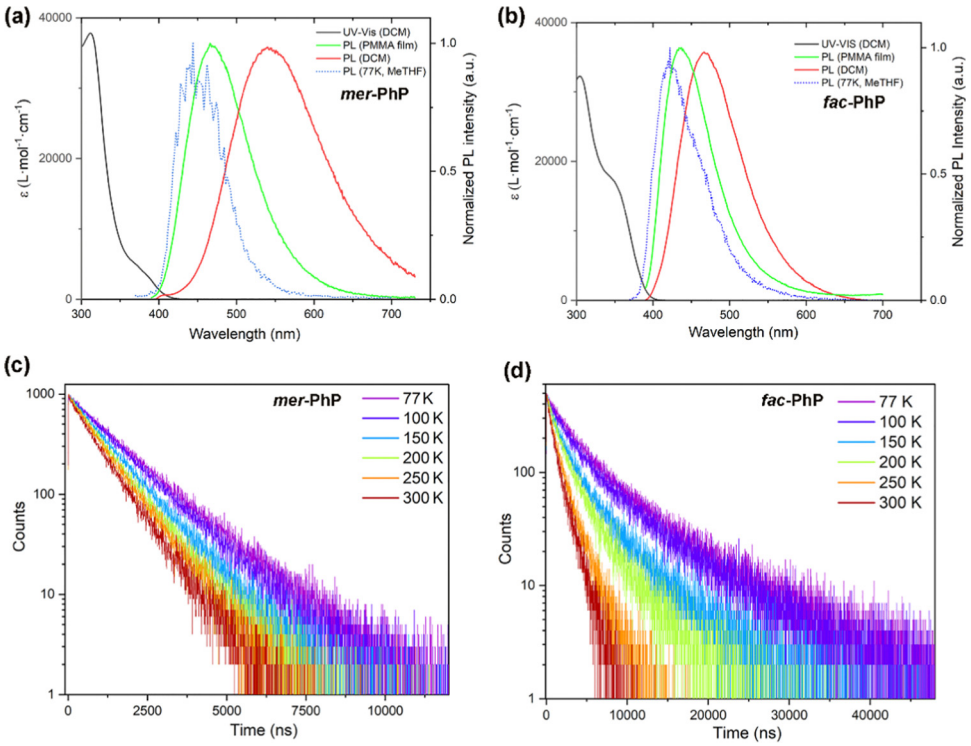

Fig. 3 UV-Vis spectra in DCM solution and PL spectra in DCM solution, PMMA films (5 wt%) and in frozen MeTHF glass at 77 K for ***mer*-PhP** (a) and ***fac*-PhP** (b). Temperature dependent PL decay curves for ***mer*-PhP** (c) and ***fac*-PhP** (d) measured in PMMA films (5 wt% emitter content).

weaker absorbing spectral features associated with the d–π* type singlet and triplet metal-to-ligand charge transfer states (^{1}MLCT and ^{3}MLCT).[39] Notably, MLCT bands for ***fac*-PhP** are more intensive than for *mer* isomer, a case that is typically encountered for structural isomers of cyclometalated Ir(III) complexes.[20,21,40] Another common observation is a redshift of the absorption onset in the case of ***mer*-PhP**.

Photoluminescence (PL) characteristics of the compounds were investigated using DCM and TOL solutions as well as films of 5 wt% solid solutions in PMMA and bulk PS. In all cases the compounds show a broad and featureless PL spectral profile. In DCM solution the PL band maximum is at 540 nm for ***mer*-PhP** and 466 nm for ***fac*-PhP**, while in less polar TOL both compounds possess blueshifted emission with PL maxima at 492 and 436 nm, respectively. The change of medium also influences the width of the PL bands, as in DCM the full width at half maximum (FWHM) is substantially increased (by 56 nm for ***mer*-PhP** and by 28 nm for ***fac*-PhP**). It is also apparent that in both solvents ***mer*-PhP** shows significantly larger FWHM in comparison to its stereoisomer. For iridium(III) complexes PL band broadening is indicative of a greater deviation between ground (S_0) and excited triplet (T_1) state geometries and suggests increased conformational uncertainty of the corresponding structures.[41,42] To support this assumption time-wavelength resolved maps of ***mer*-PhP** emission for TOL solution covering the first 50 ns after excitation was obtained at room temperature and at 77 K (Fig. 4). Striking difference can be seen between the two measurements, as under room temperature conditions dynamic red displacement of the emission band with a peak maxima shift from 470 to 520 nm can be seen. In the frozen sample the emission wavelength is almost static and resides at about 470 nm. It can be concluded that for ***mer*-PhP** a transfer between two local minima on the T_1 state potential energy surface becomes possible upon thermal activation or during the transfer from rigid to liquid surrounding medium. The role of the surrounding matrix rigidity is also underlined by PL measurements for PMMA and PS polymer guest–host systems, where ***mer*-PhP** shows emission wavelength values that are comparable to the frozen TOL sample (Table 1).

In DCM solutions the compounds show relatively low photoluminescence quantum yields (Φ_{PL}). The values of 0.12 and 0.36 were observed for DCM solutions of ***mer*-PhP** and ***fac*-PhP** respectively. In TOL solutions the emission efficiency substantially increases for ***mer*-PhP** reaching a value of 0.40, while for its isomer it drops to 0.22. In the first case the observation can be reasoned with the energy gap law, where a blueshift in emission leads to higher Φ_{PL}.[43] The lower quantum yield for ***fac*-PhP** can be explained by the poor solubility of the compound in TOL, which may lead to aggregation induced emission quenching. The poorer solubility of *fac*-isomer can be related to a higher polarity of the complex, which is indicated by the calculated dipole moment parameter for the molecule: 6.9 D *vs.* 4.4 D for the *mer*-counterpart. The Φ_{PL} substantially increases for the films of the solid solutions in PMMA, where *fac*-isomer shows the value of 0.77, while *mer*- has a value of 0.99. Again, this points to substantial differences in the degree of complex conformational freedom between DCM and the rigid solid-state host, as in liquid solution molecular geometries associated with rapid non-radiative pathways may be accessible, while in films these conformations are not attainable due to

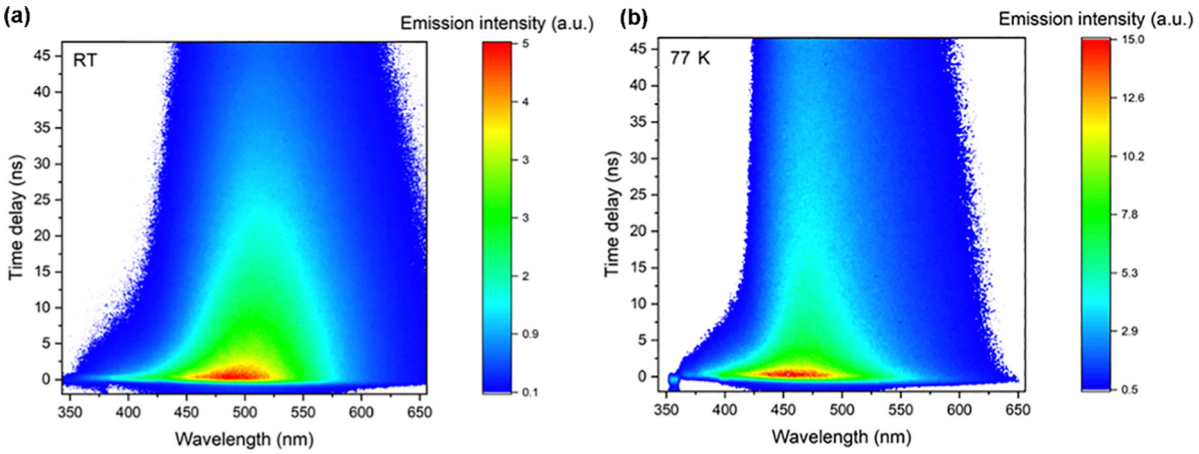

Fig. 4 Time-wavelength resolved emission intensity maps of toluene solutions of ***mer*-PhP** at a 50 ns timescale at room temperature (a) and 77 K (b).

restricted structural motion.[44] Notably, the non-radiative relaxation can also be induced in a solid host by heating

PL kinetics of the compounds were investigated by employing time-resolved photoluminescence measurements (Fig. 3c, d . In deoxygenated DCM the compounds show monoexponential PL decays with lifetimes (τ) of 353 and 532 ns for ***mer*-PhP** and ***fac*-PhP** respectively. These values fall in a typical emission lifetime range observed for cyclometalated Ir(III) complexes and are indicative of a rapid phosphorescence form T_1 state enabled by a heavy atom effect.[5,7] Temperature dependent PL decay measurements were performed for the films of doped PMMA, covering the temperature range 300–77 K (Fig. 3c, d). While the PL decay profile for ***mer*-PhP** retains its monoexponential character, the film sample of ***fac*-PhP** requires a double exponential fit. This particular behavior of ***fac*-PhP** can be presumably explained by a partial aggregation of the more polar emitter molecules or specific polymer–complex interactions, which gives rise to an additional population of emissive species. Notably, in a less polar PS host ***fac*-PhP** exhibits monoexponential decay. This points to a polymer–complex interaction being the reason for double exponential PL decay in PMMA due to the presence of a highly polar ester group, which can facilitate dipolar interactions between guest and host molecules and alter the emissive properties of the emitter. Another notable observation for the examined film samples is a substantial difference in radiative rate constants (k_r) between the two compounds. ***mer*-PhP** shows about twofold higher radiative rate constant in comparison to ***fac*-PhP**. With cooling, both compounds exhibit a slight PL lifetime increase. This is a characteristic behavior of phosphorescent iridium(III) complexes and is related to considerable zero-field splitting between the sublevels of the triplet state and the associated thermal activation of the emissive process.[44]

Computational analysis

A series of DFT calculations were performed. Geometry optimizations were carried at the PBE0, LACVP** level. The calculated ground-state structures are in good agreement with the experimental X-ray data . Ground state molecular orbital distribution and TD-DFT excitation calculations were performed

In order to describe the phosphorescence process TD-DFT calculations were performed at optimized T_1 geometries. NTO distributions for the $S_0 \rightarrow T_1$ transition are fairly similar to the lowest energy singlet excitation and indicate an MLCT character. It should be noted that the geometries of the compounds undergo substantial transformations, evident by the metal–ligand bond length changes . For ***fac*-PhP** this causes a loss of C_3 symmetry, and as a result, the electron transition in the T_1 state for both complexes proceeds predominantly between the metal d orbital and one of the attached purine rings. Interestingly, in the case of ***mer*-PhP** the ligand, which is involved in charge transfer and hosts through a MLCT process excited electron, shifts further away from the central metal atom due to a significant elongation of metal–carbene bond Ir–C1 (Ir–C1 changes from 2.04 to 2.15 Å, while Ir–C2 changes from 2.11 to 2.10 Å). This is a contrasting behavior to some conventional iridium(III) emitters, *e.g.* $Ir(ppy)_3$, for which an opposite trend is observed – in the T_1 state the electron-hosting ligand moves closer to the metal.[45,46] ***fac*-PhP** demonstrates an in-between case, as for the electron-hosting ligand the length of the metal-purine bond increases, while the phenyl–metal bond shortens (Ir–C1 changes from 2.01 to 2.06 Å, while Ir–C2 changes from 2.10 to 2.06 Å). Since an increased interatom distance can be related with a lower bonding strength and higher susceptibility to structural transformations, the predicted T_1 geometry of ***mer*-PhP** may explain the previously described observations regarding its PL behavior, where the compound exhibited a dynamic shift in PL wavelength and high sensitivity to the surrounding medium polarity and viscosity. Partial or full dissociation of ligands is one of the proposed structural transformation pathways of excited cyclometalated iridium(III) complex molecules and would be more pronounced in the case of *mer*-isomer.[47,48] The calculated T_1 energies of ***mer*-PhP** and ***fac*-PhP** are 2.60

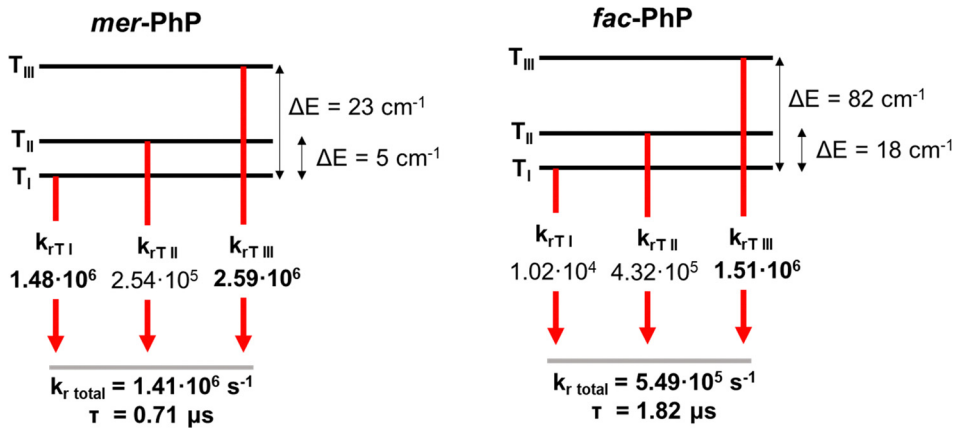

Fig. 5 Triplet sublevel configuration of the T_1 state of the synthesized complexes. Energy differences and radiative rates for individual sublevels are given. The total emissive rate is calculated at a temperature of 300 K.

and 2.93 eV (476 and 423 nm), respectively, and correspond well with the experimentally observed phosphorescence band maxima in PMMA films.

SOC-TD-DFT calculations were performed to better characterize the emissive triplet excited state of the synthesized complexes (Fig. 5). For ***mer*-PhP** two of the three triplet sublevels (T_I and T_{III}) show fast radiative rates. In contrast, only T_{III} possesses a comparable emissive k_r value for ***fac*-PhP**. A three level Boltzmann relationship was applied to calculate the total emissive rate of the complexes at 300 K temperature.[49] The obtained values of 1.41×10^6 and 5.49×10^5 s^{-1} for ***mer*-PhP** and ***fac*-PhP**, respectively, are in close agreement with the experimental observations in PMMA film samples. A significant increase in k_r for *mer*-isomer can be, at least partly, explained by the slightly larger MLCT related HOMO-to-LUMO electron transition contribution towards the $S_0 \rightarrow T_1$ excitation, amounting to 95% (in comparison to 89% in the case of *fac*-isomer). Another notable observation is the increased predicted zero-field splitting in the case of ***fac*-PhP**. This provides an explanation of the more pronounced cooling-induced PL lifetime increase in the case of *fac*-isomer (Fig. 3d).

Charge-transporting properties

For the investigation of the charge-transporting properties of vacuum-deposited layers of ***mer*-PhP** and ***fac*-PhP** we used the time-of-flight (TOF) method at room temperature.[50] The ITO/***mer*-PhP** or ***fac*-PhP** samples were used for the measurements of the TOF photocurrent. The layer thicknesses (d) were 1043 nm for ***mer*-PhP** and 1475 nm for ***fac*-PhP**. The photocurrent charge carrier transients were measured under different electric fields (E) by applying a positive or negative voltage (V) to ITO. During the measurements carried out by applying a positive voltage at ITO, it was possible to detect the transit times (t_{tr}) for holes (Fig. 6a and b). The transition times for electrons were not observed . This implies that ***mer*-PhP** and ***fac*-PhP** only transport holes. The hole mobility (μ_h) values were calculated using the formula $\mu_h = d^2/(V \times t_{tr})$.[50] They are plotted as a function of the electric field in Fig. 6c. The electric field hole mobility dependences of ***mer*-PhP** and ***fac*-PhP** were well-fitted by the formula $\mu_h = \mu_0 \times \exp(\beta \times E^{1/2})$ expressing the Poole–Frenkel electric field dependence.[51] The values of zero-electric-field mobilities (μ_0) for ***mer*-PhP** and ***fac*-PhP** were obtained through the Poole–Frenkel fitting. The obtained values of μ_o were found to be of 2.95×10^{-6} cm^2 V^{-1} s^{-1} and 2×10^{-4} cm^2 V^{-1} s^{-1}, respectively. Field dependence parameters (β) were also obtained through the same process. The values of β were found to be 3.77×10^{-3} $cm^{1/2}$ $V^{-1/2}$ and 1.22×10^{-3} $cm^{1/2}$ $V^{-1/2}$ for ***mer*-PhP** and ***fac*-PhP**, respectively. The TOF measurements demonstrate that changing the isomers of homoleptic purine-based NHC iridium(III) complexes has a strong effect on the hole-transporting properties

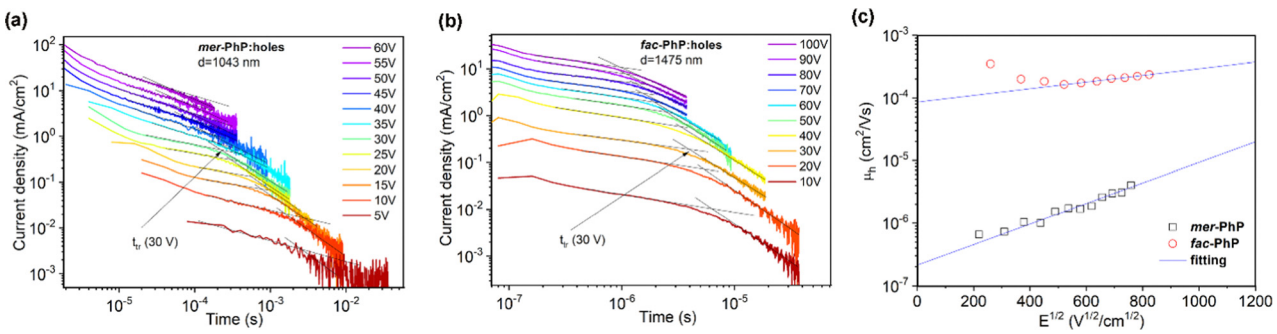

Fig. 6 TOF transients for holes for the layers of ***mer*-PhP** (a) and ***fac*-PhP** (b) recorded at different voltages applied to ITO. Electric field hole mobility dependencies of ***mer*-PhP** and ***fac*-PhP** (c). The values of t_{tr} were obtained as demonstrated by the arrows in (a) and (b).

of the tested complexes. Meanwhile, the different hole-transporting properties of ***mer*-PhP** and ***fac*-PhP** may result in varied electronic device output parameters, as discussed in the following section.

Electrophosphorescence

Electrophosphorescent properties of the complexes were studied by selecting the following initial PhOLED structure: ITO/MoO_3(0.3 nm)/NPB(36 nm)/TCTA(4 nm)/mCP(4 nm)/emitting layer (EML)(24 nm)/TSPO1(4 nm)/TPBi(40 nm)/LiF/Al. Due to the exceptional thermal stability of the compounds, the devices could be fabricated using a vacuum deposition technique. Commonly used commercial materials, *i.e.*, molybdenum oxide (MoO_3), *N*,*N*′-di(1-naphthyl)-*N*,*N*′-diphenyl-(1,1′-biphenyl)-4,4′-diamine (NPB), tris(4-carbazoyl-9-ylphenyl)amine (TCTA), 1,3-bis(9-carbazolyl)benzene (mCP), diphenyl-4-triphenylsilylphenylphosphineoxide (TSPO1), 2,2′,2″-(1,3,5-benzinetriyl)-tris(1-phenyl-1-*H*-benzimi-dazole) (TPBi) and lithium fluoride (LiF) were selected as functional materials for multi-layered PhOLED. The selected materials were used for deposition of the hole and electron injecting layers (MoO_3 and LiF), hole and electron transporting layers (NBB/TCTA and TPBi), exciton, hole and electron blocking layers (mCP and TSPO1). Taking into account its higher solid-state Φ_{PL} value, ***mer*-PhP** was initially selected as the emitter. The devices named A, B and C incorporated EMLs with 1, 5 or 10 wt% of emitter molecularly dispersed in the mCP host material. For benchmarking purposes a reference device (R) with 5 wt% of conventional blue emitter bis[2-(4,6-difluorophenyl)pyridinato-C2,*N*](picolinato)-iridium (FIrpic)[10] was fabricated. The obtained output characteristics of the devices (Table 2) show that the optimal concentration of ***mer*-PhP** is 5 wt%.

Further optimization was attempted by preparing devices D–G. We investigated how the nature of hosts (DPEPO and BCPO) affects the electroluminescent properties of ***mer*-PhP** and ***fac*-PhP**. The architecture of the devices was as follows: ITO/HAT-CN(10 nm)/TAPC(32 nm)/TCTA(10 nm)/EML (24 nm)/TSPO1 (4 nm)/TPBi(40 nm)/LiF/Al, where 1,4,5,8,9,11-hexaazatriphenylenehexacarbonitrile (HATCN) is the hole-injecting material, TCTA and 1,1-bis[(di-4-tolylamino)phenyl]cyclohexane (TAPC) are the hole-transporting materials, and bis[2-(diphenylphosphino)phenyl]ether oxide (DPEPO), or bis-4-(*N*-carbazolyl)phenyl)phenylphosphine oxide (BCPO) are EML hosts. The selection of hosts was mainly reasoned with their triplet levels, charge-injecting and charge-transporting properties, which fit well with that of ***mer*-PhP**. For example, triplet levels (2.9 eV for mCP,[52] 2.99 eV for DPEPO[53] and 3.01 eV for BCPO[54]) are close to that of ***mer*-PhP** (3.02 eV). Equilibrium energy diagrams of the investigated devices are given in Fig. 7. The ionisation potentials (IP^{PE}) of the emitters were determined by photoelectron emission spectroscopy in air, yielding the values of 5.60 and 5.81 eV observed for ***mer*-PhP** and ***fac*-PhP** respectively . The electron affinity (EA^{PE}) of 2.46 and 2.77 eV was calculated for ***mer*-PhP** and ***fac*-PhP** respectively by the formula $EA^{PE} = IP^{PE} - E_g$. Here E_g is the optical band gap taken from the edge of the absorption spectra. For ***mer*-PhP** and ***fac*-PhP** the E_g values were found to be of 3.14 and 3.04 eV, respectively (Fig. 3a and b). MoO_3/NPB/TCTA/mCP and HAT-CN/TAPC/TCTA architectures were used to provide good hole transport and injection into EML by minimising the energy barrier between the anode and HOMO of the guest and host. With the same logic the layers of TSPO1/TPBi/LiF were used for efficient and barrier-free electron transport from the cathode. Consequently, there were no interlayer energy barriers higher than 0.3 eV (Fig. 7). In addition, high triplet levels of mCP (2.9 eV),[52] TCTA (2.8 eV)[55] and TSPO1 (3.36 eV)[56] were meant to block triplets within the EML and to localize their emissive relaxation.

In agreement with the above assumption, the electroluminescence (EL) in devices A–E mainly originates from ***mer*-PhP** (Fig. 8a). EL spectra of devices A and C are supplemented with low-intensity high-energy bands related to the host emission and indicate nonoptimal concentration of the guest. Depending on the device architecture the EL maxima range from 467 to 493 nm. These shifts in EL spectra can be attributed to the solvatochromic response of ***mer*-PhP** to the different host materials. The best performing OLED shows stable EL spectra with a maximum at 467 nm without any deviations or host emissions throughout the applied voltage range (Fig. 8a). In contrast, the EL spectra of the reference device R undergo notable voltage-dependent changes , which is a typical bahaviour for FIrpic-based OLEDs.[57] In comparison to the close structural analogue *m*-2*t*Bu (device L2),[21] ***mer*-PhP** exhibits notably blue-shifted EL (467 *vs.* 482 nm). This difference in EL spectra can be explained

Table 2 Output electrophosphorescence parameters of devices A–G and R

Device	**EML**	λ, nm	V_{ON}[a], V	L_{MAX}[b], cd m^{-2}	CE_{MAX}[c], cd A^{-1}	PE_{MAX}[d], lm W^{-1}	EQE_{MAX}[e], %
Structure: ITO/MoO_3/NPB/TCTA/mCP/**EML**/TSPO1/TPBi/LiF/Al							
A	***mer*-PhP** (1 wt%):mCP	492	4	870	7.6	3.9	4.3
B	***mer*-PhP** (5 wt%):mCP	493	4.5	6320	22.3	13.5	11
C	***mer*-PhP** (10 wt%):mCP	494	5.1	2700	13.1	7.3	6.3
R	FIrpic (5%):mCP	471; 492	3.9	15 070	32	21.6	14.3
Structure: ITO/HATCN/TAPC/TCTA/**EML**/TSPO1/TPBi/LiF/Al							
D	***mer*-PhP** (5 wt%):DPEPO	467	4.2	4310	23.1	14.3	16.1
E	***mer*-PhP** (5 wt%):BCPO	482	3.1	29 520	17.5	11.9	8.55
F	***fac*-PhP** (5 wt%):DPEPO	443	4.8	520	3	1.4	3.4
G	***fac*-PhP** (5 wt%):BCPO	416	4.2	155	0.28	0.12	0.42

[a] Voltage, at which a luminance of 1 cd m^{-2} was reached. [b] Maximal attained luminance. [c] Maximal current efficiency. [d] Maximal power efficiency. [e] Maximal external quantum efficiency.

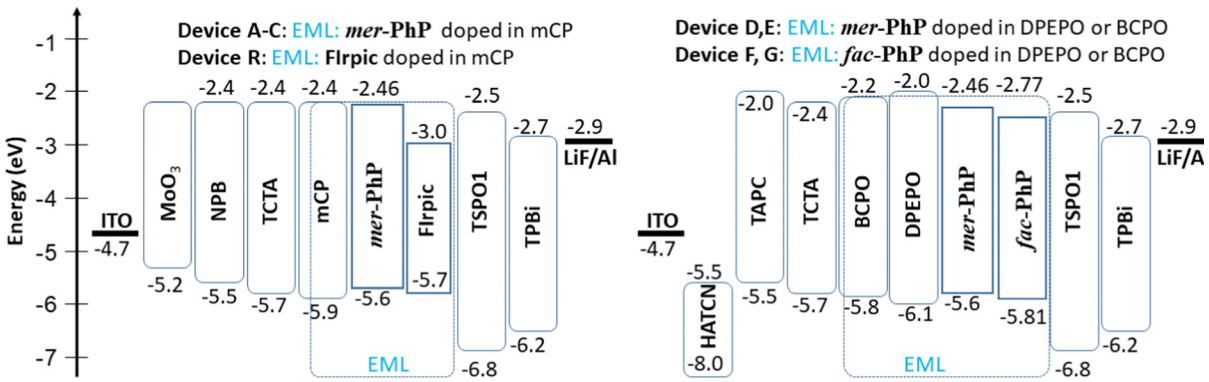

Fig. 7 Equilibrium energy diagrams of devices A–G and R.

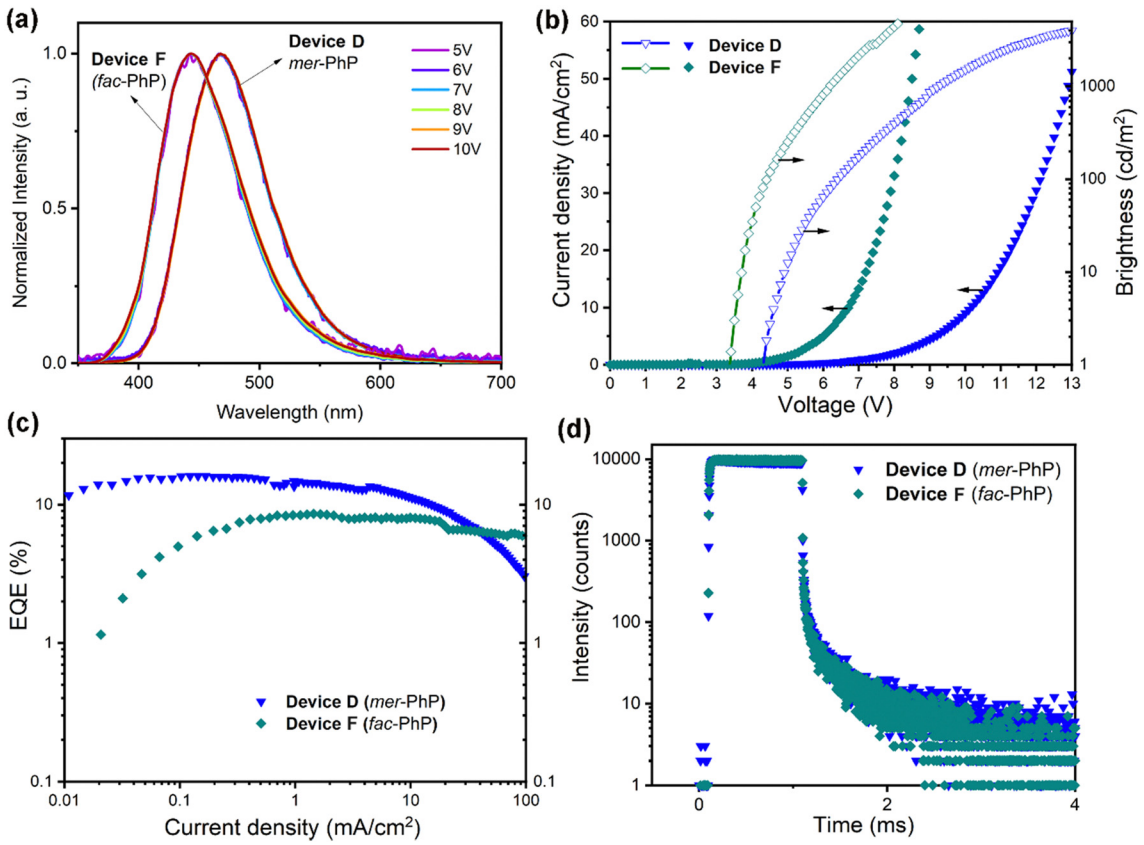

Fig. 8 EL spectra recorded at different driving voltages (a), plots of current density and brightness *versus* external voltage (b), plot of EQE *versus* current density (c), and EL decay curves (d) of ***mer*-PhP**-based device D and ***fac*-PhP**-based device F.

by the weak electron donating properties of *tert*-butyl substituents in *m*-2*t*Bu.

The onsets of electrophosphorescence (at 1 cd m^{-2}) for A–E are observed at the voltages of 3.1–5 V, which are relatively low values for blue OLEDs (Fig. 8b). The use of hosts with different HOMO and LUMO and charge-transporting properties allows tunning of the hole–electron balance within the EML of the devices . This tunning manifests as the difference in current density and brightness-*versus*-voltage characteristics. Notably, the lowest current density is observed for the best performing device D, indicating the most efficient charge carrier balance in EML. The maximum brightness of 29 520 cd m^{-2} is attained for device E. This result can apparently be attributed to the highest T_g value of the applied host material BCPO (137 °C)[54] in comparison to those of mCP (60 °C)[58] and DPEPO (93 °C).[59] The maximum brightness of device E considerably exceeds that achieved for the reference devices L1–L4 .

The highest external quantum efficiency (EQE) of 16.1% is achieved for device D, using DPEPO as the host material (Fig. 8c and Table 2). Hole–electron pairs recombine on ***mer*-PhP** since its HOMO (−5.6 eV) and LUMO (−2.46 eV) values are situated within the band gap of DPEPO with the HOMO (−6.1 eV) and LUMO (−2.0 eV) (Fig. 7). The difference in performance of the different hosts is hard to explain. Most likely it is related to the peculiarities of the charge transporting properties of the corresponding materials. In terms of overall characteristics OLEDs based on emitter ***mer*-PhP** are comparable to the reference devices L1–L4 .

The transient electroluminescence (TREL) signals were recorded for devices D and F, providing additional information on the carrier balance and charge-trapping in EML (Fig. 8d). The TREL signals are characterised by at least two EL components, a dominating microsecond component and a lower-intensity millisecond component. The microsecond component is related to the phosphorescence of ***mer*-PhP**. The millisecond component can be associated to the transport of the trapped charge carriers.[60–62] However, the typical signal (spikes)[61] for detrapped charges with the following recombination at the moment of turn-off is not observed. Thus, the millisecond time component is most likely caused by long-lived triplet excitons of the host molecules before their transfer to the guest and the following emissive relaxation. Overall, the observed TREL signals for D and E are characteristic for devices with a balanced hole and electron ratio in the EML.[63,64]

In addition, devices F and G were fabricated using complex ***fac*-PhP** as the emitter and employing the previously optimized architecture ITO/HATCN/TAPC/TCTA/***fac*-PhP** (5 wt%):DPEPO or BCPO/TSPO1/TPBi/LiF/Al. The measured characteristics are outlined in Fig. 8 . In accordance to the previous PL measurements the observed EL maximums are blue-shifted in relation to the *mer* isomer-based devices. The performance characteristics for ***fac*-PhP** are notably lower with the attained EQE value for the best performing device F at only 3.4%. This observation can be partly explained by the high triplet energy level of the emitter (3.22 eV), which is not compatible with that of the applied host material. In addition, the highly contrasting shape of the current density *versus* external voltage plots for ***mer*-PhP**- and ***fac*-PhP**-based devices indicate significant differences in charge-transporting properties of the emissive layers (Fig. 8b). Both complexes showed the best electroluminescent performance (reaching EQEs of 16.1 and 3.4%, respectively) when DPEPO was used as the host. They demonstrated much lower EQEs when BCPO was used. The high hole mobility of the host and/or guest may lead to an electron and hole disbalance in light-emitting layers of devices. In our case, the electron mobility of 1.96×10^{-6} cm^2 V^{-1} s^{-1} for DPEPO[65] is very similar to the hole mobility values of ***mer*-PhP** allowing optimal hole–electron balance within the light emitting layer of device D. Device F showed a maximum EQE of only 3.4% despite the relatively high PLQY of the emitter used. This may be attributed to the significant difference between the hole mobility of ***fac*-PhP** (2×10^{-4} cm^2 V^{-1} s^{-1}) and electron mobility of DPEPO (Fig. 6c).

Conclusions

In this work we have successfully developed a synthetic methodology towards iridium(III) complexes bearing unsubstituted 7,9-dihydro-8*H*-purin-8-ylidene ligands. The acquired phosphorescent emitters ***mer*-PhP** and ***fac*-PhP** possess exceptional thermal stability and combine high Φ_{PL} values of up to 0.99 with sub-microsecond emission lifetimes. Photophysical behavior varies significantly between the investigated *mer*- and *fac*-isomers. In polymer films ***mer*-PhP** exhibits a higher PL efficiency and significantly faster radiative rate. On the other hand, the compound shows higher sensitivity towards external stimulus, where Φ_{PL} significantly drops in response to either heating or transfer from rigid to fluid surrounding medium. DFT calculations relate this to weakened metal–ligand bonding in the T_1 excited state of ***mer*-PhP**, which may facilitate the probability of non-radiative relaxation pathways. This highlights some additional aspects that need to be taken into consideration during OLED preparation that are often neglected, such as the rigidity of the EML host material and temperature changes in operational devices. In addition, *mer*- and *fac*-isomers exhibit highly contrasting charge-transporting properties with hole mobility values of 2.95×10^{-6} cm^2 V^{-1} s^{-1} and 2×10^{-4} cm^2 V^{-1} s^{-1} at an electric field of 4.9×10^5 V cm^{-1}, resulting in a notable difference in OLED performance. In OLEDs ***mer*-PhP** is the best performing emitter, characterized by blue electroluminescence peaking at 467 nm and an external quantum efficiency of 16.1% in this way demonstrating that the presented structural design is well suited for the development of promising blue phosphorescent materials.

Conflicts of interest

There are no conflicts of interest to declare.

Acknowledgements

KT acknowledges funding by M-era.Net as part of project Eco-OLED: ≪Enabling a Commercially Viable Long Lifespan and High-Efficiency Omni-Friendly OLED Lighting Source with G2 and G3 Emitters≫, contract No. ES RTD/2020/13. AS, IN, MT, and GJ acknowledge PHC Osmose (project #48351ZC (for France) and #LV-FR/2023/2 (for Latvia)) for financial support of scientific exchanges. IN and MT thank the Latvia-Lithuania-Taiwan joint grant "Molecular Electronics in functionalized Purines: fundamental Study and applications (MEPS)" for financial support. This work has received funding from the Research Council of Lithuania (LMTLT), agreement No S-MIP-23-50.

References

1 G. Hong, X. Gan, C. Leonhardt, Z. Zhang, J. Seibert, J. M. Busch and S. Bräse, A Brief History of OLEDs—Emitter Development and Industry Milestones, *Adv. Mater.*, 2021, **33**, 2005630.

2 H.-W. Chen, J.-H. Lee, B.-Y. Lin, S. Chen and S.-T. Wu, Liquid crystal display and organic light-emitting diode display: present status and future perspectives, *Light Sci. Appl.*, 2018, **7**, 17168.

3 S. Park, J. T. Lim, W.-Y. Jin, H. Lee, B.-H. Kwon, N. S. Cho, J.-H. Han, J.-W. Kang, S. Yoo and J.-I. Lee, Efficient Large-Area Transparent OLEDs Based on a Laminated Top Electrode with an Embedded Auxiliary Mesh, *ACS Photonics*, 2017, **4**, 1114–1122.

4 C. Il Park, M. Seong, M. A. Kim, D. Kim, H. Jung, M. Cho, S. H. Lee, H. Lee, S. Min, J. Kim, M. Kim, J.-H. Park, S. Kwon, B. Kim, S. J. Kim, W. Park, J.-Y. Yang, S. Yoon and I. Kang, World's first large size 77-inch transparent flexible OLED display, *J. Soc. Inf. Disp.*, 2018, **26**, 287–295.

5 S. Lamansky, P. Djurovich, D. Murphy, F. Abdel-Razzaq, H.-E. Lee, C. Adachi, P. E. Burrows, S. R. Forrest and M. E. Thompson, Highly Phosphorescent Bis-Cyclometalated Iridium Complexes: Synthesis, Photophysical Characterization, and Use in Organic Light Emitting Diodes, *J. Am. Chem. Soc.*, 2001, **123**, 4304–4312.

6 C. Ulbricht, B. Beyer, C. Friebe, A. Winter and U. S. Schubert, Recent Developments in the Application of Phosphorescent Iridium(III) Complex Systems, *Adv. Mater.*, 2009, **21**, 4418–4441.

7 H. Yersin, A. F. Rausch, R. Czerwieniec, T. Hofbeck and T. Fischer, The triplet state of organo-transition metal compounds. Triplet harvesting and singlet harvesting for efficient OLEDs, *Coord. Chem. Rev.*, 2011, **255**, 2622–2652.

8 T.-Y. Li, J. Wu, Z.-G. Wu, Y.-X. Zheng, J.-L. Zuo and Y. Pan, Rational design of phosphorescent iridium(III) complexes for emission color tunability and their applications in OLEDs, *Coord. Chem. Rev.*, 2018, **374**, 55–92.

9 A. Monkman, Why Do We Still Need a Stable Long Lifetime Deep Blue OLED Emitter?, *ACS Appl. Mater. Interfaces*, 2022, **14**, 20463–20467.

10 C. Adachi, R. C. Kwong, P. Djurovich, V. Adamovich, M. A. Baldo, M. E. Thompson and S. R. Forrest, Endothermic energy transfer: A mechanism for generating very efficient high-energy phosphorescent emission in organic materials, *Appl. Phys. Lett.*, 2001, **79**, 2082–2084.

11 R. Seifert, I. Rabelo de Moraes, S. Scholz, M. C. Gather, B. Lüssem and K. Leo, Chemical degradation mechanisms of highly efficient blue phosphorescent emitters used for organic light emitting diodes, *Org. Electron.*, 2013, **14**, 115–123.

12 D. Jacquemin and D. Escudero, The short device lifetimes of blue PhOLEDs: insights into the photostability of blue Ir(III) complexes, *Chem. Sci.*, 2017, **8**, 7844–7850.

13 X. Zhou and B. J. Powell, Nonradiative Decay and Stability of N -Heterocyclic Carbene Iridium(III) Complexes, *Inorg. Chem.*, 2018, **57**, 8881–8889.

14 S. Arroliga-Rocha and D. Escudero, Facial and Meridional Isomers of Tris(bidentate) Ir(III) Complexes: Unravelling Their Different Excited State Reactivity, *Inorg. Chem.*, 2018, **57**, 12106–12112.

15 T. Sajoto, P. I. Djurovich, A. Tamayo, M. Yousufuddin, R. Bau, M. E. Thompson, R. J. Holmes and S. R. Forrest, Blue and Near-UV Phosphorescence from Iridium Complexes with Cyclometalated Pyrazolyl or N -Heterocyclic Carbene Ligands, *Inorg. Chem.*, 2005, **44**, 7992–8003.

16 A. K. Pal, S. Krotkus, M. Fontani, C. F. R. Mackenzie, D. B. Cordes, A. M. Z. Slawin, I. D. W. Samuel and E. Zysman-Colman, High-Efficiency Deep-Blue-Emitting Organic Light-Emitting Diodes Based on Iridium(III) Carbene Complexes, *Adv. Mater.*, 2018, **30**, 1804231.

17 J. Lee, H.-F. Chen, T. Batagoda, C. Coburn, P. I. Djurovich, M. E. Thompson and S. R. Forrest, Deep blue phosphorescent organic light-emitting diodes with very high brightness and efficiency, *Nat. Mater.*, 2016, **15**, 92–98.

18 A. Maheshwaran, V. G. Sree, H.-Y. Park, H. Kim, S. H. Han, J. Y. Lee and S.-H. Jin, High Efficiency Deep-Blue Phosphorescent Organic Light-Emitting Diodes with CIE x, y ($\leq$ 0.15) and Low Efficiency Roll-Off by Employing a High Triplet Energy Bipolar Host Material, *Adv. Funct. Mater.*, 2018, **28**, 1802945.

19 M. Jung, K. H. Lee, J. Y. Lee and T. Kim, A bipolar host based high triplet energy electroplex for an over 10 000 h lifetime in pure blue phosphorescent organic light-emitting diodes, *Mater. Horizons*, 2020, **7**, 559–565.

20 M. Idris, S. C. Kapper, A. C. Tadle, T. Batagoda, D. S. Muthiah Ravinson, O. Abimbola, P. I. Djurovich, J. Kim, C. Coburn, S. R. Forrest and M. E. Thompson, Blue Emissive fac/mer -Iridium (III) NHC Carbene Complexes and their Application in OLEDs, *Adv. Opt. Mater.*, 2021, **9**, 2001994.

21 J. Jin, Z. Zhu, J. Yan, X. Zhou, C. Cao, P.-T. Chou, Y.-X. Zhang, Z. Zheng, C.-S. Lee and Y. Chi, Iridium(III) Phosphors–Bearing Functional 9-Phenyl-7,9-dihydro-8H-purin-8-ylidene Chelates and Blue Hyperphosphorescent OLED Devices, *Adv. Photonics Res.*, 2022, **3**, 2100381.

22 Y. Qin, X. Yang, J. Jin, D. Li, X. Zhou, Z. Zheng, Y. Sun, W. Y. Wong, Y. Chi and S. J. Su, Facially Coordinated, Tris-bidentate Purin-8-ylidene Ir(III) Complexes for Blue Electrophosphorescence and Hyperluminescence, *Adv. Opt. Mater.*, 2022, **10**, 1–13.

23 H. U. Kim, H. J. Park, J.-H. Jang, W. Song, I. H. Jung, J. Y. Lee and D.-H. Hwang, Green phosphorescent homoleptic iridium(III) complexes for highly efficient organic light-emitting diodes, *Dyes Pigm.*, 2018, **156**, 395–402.

24 C. F. R. Mackenzie, L. Zhang, D. B. Cordes, A. M. Z. Slawin, I. D. W. Samuel and E. Zysman-Colman, Bulky Iridium NHC Complexes for Bright, Efficient Deep-Blue OLEDs, *Adv. Opt. Mater.*, 2023, **11**, 2201495.

25 J.-H. Kim, S.-Y. Kim, D. W. Cho, H.-J. Son and S. O. Kang, Influence of bulky substituents on the photophysical properties of homoleptic iridium(III) complexes, *Phys. Chem. Chem. Phys.*, 2019, **21**, 6908–6916.

26 A. Ruduss, V. Kokars, N. Tetervenoka, A. Vembris and K. Traskovskis, Effects of steric encumbrance of iridium(III) complex core on performance of solution-processed organic light emitting diodes, *RSC Adv.*, 2020, **10**, 27552–27559.

27 G. Zhang, F. Hermerschmidt, A. Pramanik, D. Schollmeyer, M. Baumgarten, P. Sarkar, E. J. W. List-Kratochvil and K. Müllen, Bulky, dendronized iridium complexes and their photoluminescence, *J. Mater. Chem. C*, 2019, **7**, 15252–15258.

28 A. Laxer, H. E. Gottlieb and B. Fischer, Molecular recognition of adenosine deaminase: 15N NMR studies, *Nucleosides, Nucleotides Nucleic Acids*, 2007, **26**, 161–180.

29 A. Vik, E. Hedner, C. Charnock, L. W. Tangen, Ø. Samuelsen, R. Larsson, L. Bohlin and L. L. Gundersen, Antimicrobial and cytotoxic activity of agelasine and agelasimine analogs, *Bioorganic Med. Chem.*, 2007, **15**, 4016–4037.

30 K. Leškovskis, J. M. Ząkis, I. Novosjolova and M. Turks, Applications of Purine Ring Opening in the Synthesis of Imidazole, Pyrimidine, and New Purine Derivatives, *Eur. J. Org. Chem.*, 2021, 5027–5052.

31 K. Traskovskis, A. Sebris, I. Novosjolova, M. Turks, M. Guzauskas, D. Volyniuk, O. Bezvikonnyi, J. V. Grazulevicius, A. Mishnev, R. Grzibovskis and A. Vembris, All-organic fast intersystem crossing assisted exciplexes exhibiting submicrosecond thermally activated delayed fluorescence, *J. Mater. Chem. C*, 2021, **9**, 4532–4543.

32 A. Senthilvelan, M. Shanmugasundaram and A. R. Kore, Highly regioselective methylation of inosine nucleotide: an efficient synthesis of 7-methylinosine nucleotide, *Nucleosides, Nucleotides Nucleic Acids*, 2020, **39**, 1011–1019.

33 M. L. Read, M. Braendvang, P. O. Miranda and L.-L. Gundersen, Synthesis and biological evaluation of pyrimidine analogs of antimycobacterial purines, *Bioorg. Med. Chem.*, 2010, **18**, 3885.

34 A. Sebris, I. Novosjolova and M. Turks, Synthesis of 7-Arylpurines from Substituted Pyrimidines, *Synthesis*, 2022, 5529–5539.

35 L. De Cola, S. Dueck, R. Cysewski, M. D. Galvez Lopez and J.-P. Catinat, *Novel transition metal complexes comprising symmetric tetradentate ligands*, *Ep. Pat.*, 12182638 A, 2012.

36 J. G. Osiak, T. Setzer, P. G. Jones, C. Lennartz, A. Dreuw, W. Kowalsky and H. H. Johannes, Twist it! the acid-dependent isomerization of homoleptic carbenic iridium(III) complexes, *Chem. Commun.*, 2017, **53**, 3295–3298.

37 C. Yang, F. Mehmood, T. L. Lam, S. L.-F. Chan, Y. Wu, C.-S. Yeung, X. Guan, K. Li, C. Y.-S. Chung, C.-Y. Zhou, T. Zou and C.-M. Che, Stable luminescent iridium(III) complexes with bis(N-heterocyclic carbene) ligands: photostability, excited state properties, visible-light-driven radical cyclization and CO_2 reduction, and cellular imaging, *Chem. Sci.*, 2016, **7**, 3123–3136.

38 A. B. Tamayo, B. D. Alleyne, P. I. Djurovich, S. Lamansky, I. Tsyba, N. N. Ho, R. Bau and M. E. Thompson, Synthesis and Characterization of Facial and Meridional Tris-cyclometalated Iridium(III) Complexes, *J. Am. Chem. Soc.*, 2003, **125**, 7377–7387.

39 P. J. Hay, Theoretical Studies of the Ground and Excited Electronic States in Cyclometalated Phenylpyridine Ir(III) Complexes Using Density Functional Theory, *J. Phys. Chem. A*, 2002, **106**, 1634–1641.

40 Y. Qin, X. Yang, J. Jin, D. Li, X. Zhou, Z. Zheng, Y. Sun, W. Wong, Y. Chi and S. Su, Facially Coordinated, Tris -bidentate Purin-8-ylidene Ir(III) Complexes for Blue Electrophosphorescence and Hyperluminescence, *Adv. Opt. Mater.*, 2022, **10**, 2201633.

41 X. Li, Y.-Z. Shi, K. Wang, M. Zhang, C.-J. Zheng, D.-M. Sun, G.-L. Dai, X.-C. Fan, D.-Q. Wang, W. Liu, Y.-Q. Li, J. Yu, X.-M. Ou, C. Adachi and X.-H. Zhang, Thermally Activated Delayed Fluorescence Carbonyl Derivatives for Organic Light-Emitting Diodes with Extremely Narrow Full Width at Half-Maximum, *ACS Appl. Mater. Interfaces*, 2019, **11**, 13472–13480.

42 C. Cao, J. Tan, Z. Zhu, J. Lin, H. Tan, H. Chen, Y. Yuan, M. Tse, W. Chen and C. Lee, Intramolecular Cyclization: A Convenient Strategy to Realize Efficient BT.2020 Blue Multi-Resonance Emitter for Organic Light-Emitting Diodes, *Angew. Chem., Int. Ed.*, 2023, **62**, e202215226.

43 R. Englman and J. Jortner, The energy gap law for radiationless transitions in large molecules, *Mol. Phys.*, 1970, **18**, 145–164.

44 T. Sajoto, P. I. Djurovich, A. B. Tamayo, J. Oxgaard, W. A. Goddard and M. E. Thompson, Temperature Dependence of Blue Phosphorescent Cyclometalated Ir(III) Complexes, *J. Am. Chem. Soc.*, 2009, **131**, 9813–9822.

45 X. Li, B. Minaev, H. Ågren and H. Tian, Theoretical Study of Phosphorescence of Iridium Complexes with Fluorine-Substituted Phenylpyridine Ligands, *Eur. J. Inorg. Chem.*, 2011, 2517–2524.

46 E. Jansson, B. Minaev, S. Schrader and H. Ågren, Time-dependent density functional calculations of phosphorescence parameters for *fac*-tris(2-phenylpyridine) iridium, *Chem. Phys.*, 2007, **333**, 157–167.

47 I. R. de Moraes, S. Scholz, B. Lüssem and K. Leo, Analysis of chemical degradation mechanism within sky blue phosphorescent organic light emitting diodes by laser-desorption/ionization time-of-flight mass spectrometry, *Org. Electron.*, 2011, **12**, 341–347.

48 I. R. de Moraes, S. Scholz, B. Lüssem and K. Leo, Role of oxygen-bonds in the degradation process of phosphorescent organic light emitting diodes, *Appl. Phys. Lett.*, 2011, **99**, 053302.

49 K. Mori, T. P. M. Goumans, E. van Lenthe and F. Wang, Predicting phosphorescent lifetimes and zero-field splitting of organometallic complexes with time-dependent density functional theory including spin–orbit coupling, *Phys. Chem. Chem. Phys.*, 2014, **16**, 14523–14530.

50 G. Bratina and E. Pavlica, Characterisation of charge carrier transport in thin organic semiconductor layers by time-of-flight photocurrent measurements, *Org. Electron.*, 2019, **64**, 117–130.

51 G. A. N. Connell, D. L. Camphausen and W. Paul, Theory of Poole-Frenkel conduction in low-mobility semiconductors, *Philos. Mag.*, 1972, **26**, 541–551.

52 R. J. Holmes, S. R. Forrest, Y.-J. Tung, R. C. Kwong, J. J. Brown, S. Garon and M. E. Thompson, Blue organic electrophosphorescence using exothermic host–guest energy transfer, *Appl. Phys. Lett.*, 2003, **82**, 2422–2424.

53 H. Xu, L.-H. Wang, X.-H. Zhu, K. Yin, G.-Y. Zhong, X.-Y. Hou and W. Huang, Application of Chelate Phosphine Oxide Ligand in Eu III Complex with Mezzo Triplet Energy Level, Highly Efficient Photoluminescent, and Electroluminescent Performances, *J. Phys. Chem. B*, 2006, **110**, 3023–3029.

54 H.-H. Chou and C.-H. Cheng, A Highly Efficient Universal Bipolar Host for Blue, Green, and Red Phosphorescent OLEDs, *Adv. Mater.*, 2010, **22**, 2468–2471.
55 S. Reineke, F. Lindner, G. Schwartz, N. Seidler, K. Walzer, B. Lüssem and K. Leo, White organic light-emitting diodes with fluorescent tube efficiency, *Nature*, 2009, **459**, 234–238.
56 S. O. Jeon, S. E. Jang, H. S. Son and J. Y. Lee, External Quantum Efficiency Above 20% in Deep Blue Phosphorescent Organic Light-Emitting Diodes, *Adv. Mater.*, 2011, **23**, 1436–1441.
57 J.-H. Lee, C.-H. Chen, B.-Y. Lin, Y.-H. Lan, Y.-M. Huang, N.-J. Chen, J.-J. Huang, D. Volyniuk, R. Keruckiene, J. V. Grazulevicius, Y.-R. Wu, M. Leung and T.-L. Chiu, Bistriazoles with a Biphenyl Core Derivative as an Electron-Favorable Bipolar Host of Efficient Blue Phosphorescent Organic Light-Emitting Diodes, *ACS Appl. Mater. Interfaces*, 2020, **12**, 49895–49904.
58 L. Xiao, Z. Chen, B. Qu, J. Luo, S. Kong, Q. Gong and J. Kido, Recent Progresses on Materials for Electrophosphorescent Organic Light-Emitting Devices, *Adv. Mater.*, 2011, **23**, 926–952.
59 B. A. Naqvi, M. Schmid, E. Crovini, P. Sahay, T. Naujoks, F. Rodella, Z. Zhang, P. Strohriegl, S. Bräse, E. Zysman-Colman and W. Brütting, What Controls the Orientation of TADF Emitters?, *Front. Chem.*, 2020, **8**, 750.
60 J. Kang, J. B. Son, G. W. Kim, S. Bae, K. S. Min, S. Sul, W. S. Jeon, J. Jang, G. S. Park, J. K. Shin, J. H. Kwon and S. K. Kim, Time-Resolved Electroluminescence Study for the Effect of Charge Traps on the Luminescence Properties of Organic Light-Emitting Diodes, *Phys. Status Solidi*, 2020, **217**, 2000081.
61 R. Liu, Z. Gan, R. Shinar and J. Shinar, Transient electroluminescence spikes in small molecular organic light-emitting diodes, *Phys. Rev. B: Condens. Matter Mater. Phys.*, 2011, **83**, 245302.
62 K. Ju Kim and T. Kim, Study on charge dynamics and recombination process via transient electroluminescence analysis in blue fluorescence organic light-emitting diodes, *J. Ind. Eng. Chem.*, 2023, **119**, 598–604.
63 T.-Y. Cheng, J.-H. Lee, C.-H. Chen, P.-H. Chen, P.-S. Wang, C.-E. Lin, B.-Y. Lin, Y.-H. Lan, Y.-H. Hsieh, J.-J. Huang, H.-F. Lu, I. Chao, M.-K. Leung, T.-L. Chiu and C.-F. Lin, Carrier transport and Recombination Mechanism in Blue phosphorescent organic Light-emitting Diode with Hosts Consisting of Cabazole-and triazole-Moiety, *Sci. Rep.*, 2019, **9**, 3654.
64 Z. Liu, W. Zheng, P. Wei, Z. Xu, D. Song, B. Qiao and S. Zhao, The improved performance and mechanism of solution-processed blue PhOLEDs based on double electron transport layers, *RSC Adv.*, 2020, **10**, 13215–13222.
65 J. Zhang, D. Ding, Y. Wei, F. Han, H. Xu and W. Huang, Multiphosphine-Oxide Hosts for Ultralow-Voltage-Driven True-Blue Thermally Activated Delayed Fluorescence Diodes with External Quantum Efficiency beyond 20%, *Adv. Mater.*, 2016, **28**, 479–485.